J. Fluid Mech. (1980), *vol.* 97, *part* 2, *pp.* 299–319
Printed in Great Britain

Low-frequency pressure fluctuations in axisymmetric turbulent boundary layers

By RONALD L. PANTON, A. L. GOLDMAN,†
Mechanical Engineering Department, The University of Texas, Austin, Texas 78712

R. L. LOWERY AND M. M. REISCHMAN‡
Mechanical and Aerospace Engineering Department, Oklahoma State University, Stillwater, Oklahoma

(Received 30 October 1978 and in revised form 23 July 1979)

Measurements of wall pressure fluctuations under a turbulent boundary layer were made on the fuselage of a sailplane. This flow offers a noise-free environment with a low free stream turbulence level. The axisymmetric boundary layer undergoes natural transition and develops in a zero pressure gradient region. Spectra of the wall pressure were found to decrease at low frequency in agreement with calculations based upon a turbulence–mean shear interaction mechanism. Velocity fluctuations at several positions within and outside the boundary layer were measured and correlated with the wall pressure. A special conditional correlation method was also employed to find the contribution of various velocity fluctuations to the wall pressure. A conditioning signal was formed based upon the signs of u and v and the turbulent–non-turbulent nature of the flow. This signal was time lagged and correlated with the wall pressure signal. It was found that in the outer portion of the boundary layer ($y/\delta > 0{\cdot}5$), irrotational motions were more highly correlated with the wall pressure than vortical motion.

1. Introduction

Pressure fluctuations in turbulence are often proposed as an important mechanism by which the outer region of a boundary layer can influence and perhaps initiate events in the wall region. In a recent review, Willmarth (1975*b*) has summarized and interpreted many of the previous experiments and theoretical models. Pressure fluctuation measurements are particularly difficult because extraneous free-stream turbulence and acoustic noise are readily measured by wall-mounted microphones. In order to avoid these problems Hodgson (1962, 1971) employed a sailplane and measured the pressures on the surface of the wing. We have also adopted this idea and for several years, first in Oklamoma and subsequently in Texas, have conduted a programme to measure the pressure and velocity fluctuations on a sailplane boundary layer.

Although sailplane experiments are much less convenient and controlled than wind tunnels, it was found that the longitudinal turbulence intensity (on a good day) would be between 0·05 and 0·1 %. This is comparable with results obtained with good wind

† Present address: Texas Technological University, Lubbock, Texas.
‡ Present address: Naval Undersea Center, San Diego, California.

0022–1120/80/4407–8520 $02.00

tunnels. The acoustic noise contributed to the boundary layer was also eliminated as a contaminating factor. This fact was verified by a microphone with a nose cone which was located in the free stream. The major disadvantage of the sailplane is that the boundary layer is not very thick and the microphone diameters are not small compared to the boundary-layer thickness. Thus the experiments were not able to measure the higher frequency components in the overlap region of the spectrum.

The first part of the test programme was directed toward measuring the spectrum of wall pressure fluctuations at a single point while simultaneously measuring the boundary-layer properties. Another set of measurements was made with an array of microphones and an x-wire velocity probe. The probe was located at several positions in the outer portion of the boundary layer and in the non-turbulent region. Hence, the pressure–velocity measurements reported herein are mainly concerned with the large-scale motions in these regions. The measurements are complementary to similar measurements made by Willmarth & Wooldridge (1962) where the velocity probe was in the inner portion of the boundary layer. The inner portion of the sailplane boundary layer was not measured because of inadequate spatial resolution of the microphone and the hot wires.

2. Test equipment and procedures

The tests were run using a Schweizer model 2-32 sailplane shown in figure 1 (plate 1). This is an all-metal, two-seat sailplane with a useful load of 490 lb; sufficient for the pilot and necessary instrumentation. Measurements were made on the flow field located on the lower portion of the fuselage just forward of the wing. This measurement location gives the best flow field for development of a zero-pressure-gradient boundary layer with natural transition. Measurement locations on the wing were rejected because of pressure gradients and the short length for boundary-layer development. In the measurement area, the lower half of the fuselage, is a 32 in. diameter circular cylinder for a length of 5 ft. The thickness of the boundary layer compared to the cylinder radius is $\delta/r \simeq \frac{1}{20}$. Previous experiments on axisymmetric cylindrical bodies have confirmed that the boundary layer does not substantially differ from a flat plate boundary layer (Bakewell 1968; Willmarth & Yang 1970). Complete cylindrical symmetry is maintained as the fuselage tapers forward to the nose cap. The axis of the nose section is canted downward at $3\frac{1}{2}^\circ$ with respect to the axis of the 32 in. cylinder section.

The batteries, power supplies, instruments and tape recording equipment were packaged into a frame that was installed in the second seat of the sailplane. The pilot controlled the experiment through remote switches mounted on the instrument panel. All data were recorded on a 14-channel instrument tape recorder which met IRIG intermediate band specifications at 30 ips. It was necessary to amplify all signals before they were recorded and this was accomplished by specially constructed integrated circuit amplifiers. The microphone and hot-wire signals were recorded on FM channels while several slow variables such as temperature, static and total pressure, were multiplexed and recorded.

In some preliminary tests the mean velocity of the boundary layer was measured with a traversing pitot tube. A motor-driven cam mechanism cycled the tube back and forth across the layer in 20 s intervals while a position transducer recorded the tube

position. The main tests may be classified into two types: tests with a single surface microphone and tests with an array of surface microphones. In the single point measurements microphone sizes of $\frac{1}{8}$, $\frac{1}{4}$, $\frac{1}{2}$, and 1 in. diameter were employed at various times. All microphones and their power supplies were manufactured by the Brüell and Kjaer company. Acoustic noise in the free stream was monitored by a $\frac{1}{2}$ in. microphone with a nose cone (B & K UA0052). This microphone was mounted $2\frac{1}{2}$ in. away from the fuselage and 8·75 in. aft of the primary microphone location. Free-stream velocity fluctuations were measured with a single hot wire mounted on a fixed probe which was 7·35 in. aft and 0·375 in. offset from the primary microphone. The free-stream hot wire was 3·75 in. from the wall and was oriented so that it responded to longitudinal velocity fluctuations. Results of these tests are presented in figures 4–9.

When an array of microphones was used they were all $\frac{1}{8}$ in. in diameter and were aligned in the flow direction. Approximately $\frac{3}{8}$ in. behind the last microphone an x-hot-film probe (Thermo-Systems Model 1241-20) was positioned so that both u and v turbulent velocity components could be measured. This probe could be located at various distances from the wall by a Disa remote traversing unit. Results from these tests are presented in figures 10–17.

Several methods of data processing were used during the course of the project. In early work, spectra were produced by the NASA Ames Research Center hybrid computer facility. Later on, Spectral Dynamics, Inc. tracking filters were employed for the spectral analysis. The pressure–pressure correlations of figure 10 were done on a small Saicor Inc. correlator (Model SAI-43A). This is a digital machine and was operated at a sampling rate of 50 kHz for 20 seconds of record. A correction to the time base was applied to account for an error in the tape recorder between the even and odd channel time bases. The timing error was measured from test signals recorded on the beginning of the tape prior to take off. Pressure–velocity correlations (figures 12, 13 and 14) and the conditional correlations (figures 16 and 17) were found using a still different process. Digital tapes of the FM flight signals were made in such a format that was compatible with The University of Texas CDC 6600 computer. The sampling rate for digitizing was 40 kHz and the correlations required 3 s of data. Special programs were developed for the direct computation of correlation coefficients as described by Bendat & Piersol (1971). Several correlations processed by the CDC were verified using the Saicor correlator.

3. Test environment

A typical test was performed early in the morning on a winter day. The glider was towed aloft and released at an altitude of 5000–8000 feet. As a rule of thumb the glider was released at least 3000 ft above the convective layer so that all runs were finished at least 1000 ft above the convective layer. It was always necessary to wait for a stable atmosphere and testing during summer months was impossible.

A sailplane, or any unpowered aircraft, has a definite angle of attack for a given indicated airspeed. This is true irrespective of altitude. Thus, tests conducted at the same indicated airspeed have the same inviscid flow and pressure distribution over the aircraft. All tests reported herein were conducted at 60 m.p.h. Although the sailplane has structural capacity for flight speeds of 150 m.p.h., the attitude of the plane changes significantly to even achieve 90 m.p.h.

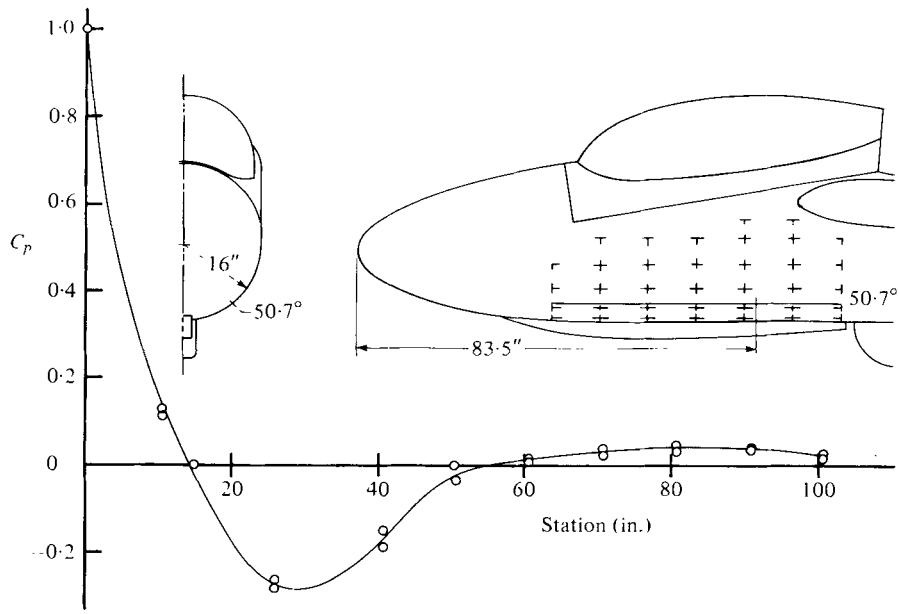

FIGURE 2. Pressure coefficient on glider surface along line 55° down from horizontal.
$C_p = (p-p_\infty)/(1/2\rho U^2)$.

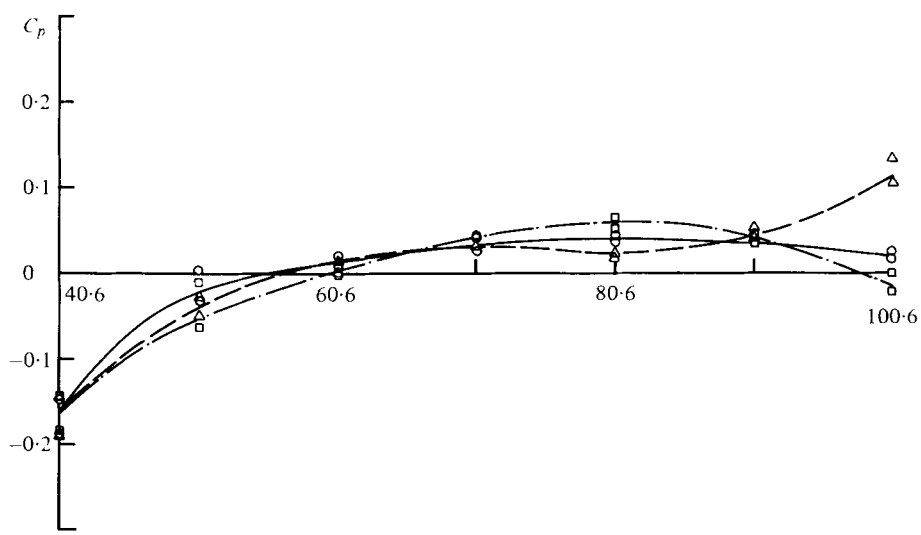

FIGURE 3. Pressure coefficient. Angle below horizontal: —·—, 35°; ——, 55°; — —, 75°.

Two preliminary studies were accomplished before choosing the measurement location and test airspeed. The surface pressure distribution was measured with an on-board manometer system and camera. Figure 2 shows the location of the pressure taps along the side of the fuselage. In the main grid the distances between taps is 5·6 × 10 in. The curves shown in figure 3 are for taps located on rows at 35°, 55° and 75° below the horizontal axis. As is typical for cylindrical bodies the pressure decreases below atmospheric and then recompresses to near the free-stream value. At the aft position

U_∞ (ft s^{-1})	δ (in.)	δ^* (in.)	H	Π	C_f	Re_δ^*	$\frac{u_* \delta}{\nu}$
100·8	0·78	0·12	1·38	0·50	$3{\cdot}25 \times 10^{-3}$	4610	1240

TABLE 1. Typical values for boundary-layer properties.

the curve for 35° shows the influence of the wing and the 75° curve shows the influence of the main landing wheel. The measurement location was selected at 50·7° down from the horizontal and at a station 83·5 in. aft of the nose. This position has a run of approximately 40 in. of nearly zero pressure gradient. The lateral extent of the field is about 10–15 in. A forward measuring position was also used to gather data on the boundary-layer growth as well as to measure the pressure fluctuations. This forward station was located at a position 60·6 in. aft of the nose.

The flow direction over the fuselage was determined by a tuft study. Motion pictures were taken from a powered plane as it flew in formation with the glider. The tuft study was most revealing and indicated that the speed range 55–65 m.p.h. was the best for having the flow aligned with the lower cylinder of the fuselage. At higher speeds the nose of the sailplane is tucked down and the flow direction is slightly across the fuselage. In this case there was some evidence of flow separation as the flow crossed from the upper fuselage on to the cylindrical lower section. Although this region is well away from the measurement location it was preferred to limit the tests to the lower speed range.

Boundary-layer profiles were measured at two locations (stations 60·6 in. and 83·5 in. from the nose). The procedure used in the Stanford Symposium by Coles & Hirst (1968) was employed to fit the data to the logarithmic law plus the wake function:

$$\frac{U}{u_*} = \frac{1}{k}\ln\left(\frac{yu_*}{\nu}\right) + C + \frac{2\Pi}{k}\sin^2\left(\frac{\pi}{2}\frac{y}{\delta}\right).$$

In this equation U is the average velocity, u_* the friction velocity, k the von Kármán constant, y the distance from the wall, ν the kinematic viscosity, C a constant, Π the wake constant and δ is the boundary-layer thickness. In Coles & Hirst's procedure $k = 0{\cdot}40$ and $C = 5{\cdot}0$ are assumed and u_*, δ and Π are computed. The resulting skin friction and wake constant agreed well with Wieghardt's wind tunnel results as quoted in the Stanford symposium (Coles & Hirst 1968, p. 98). Over the limited altitude range that was encountered there was less than a 10 % change in displacement thickness with aircraft Reynolds number. Typical values for the boundary-layer properties are shown in table 1. These values occur at the primary measuring station 83·5 in. from the nose. In order to determine the growth of the boundary layer, velocity profiles were also measured at station 60·6. Constants in the growth rate equation

$$\delta = C_1(x - x_0)^{(n+1)/(n+3)}$$

could then be determined. A shape factor of $H = 1{\cdot}4$ implies that $n = 5$ so only two measurements of δ are required to fix C_1 and x_0. The apparent origin of the boundary layer was found to be at station 45·8 or about 40 in. in front of the primary measuring position. This is also the position where the zero pressure gradient begins.

4. Pressure results

The equation which governs pressure fluctuations in a boundary layer may be written as

$$\nabla^2 p = -2\rho \frac{\partial u_2}{\partial x_1}\frac{dU_1}{dx_2} - \rho \frac{\partial^2}{\partial x_i \partial x_j}(u_i u_j - \overline{u_i u_j}).$$

In this equation $U_1(x_2)$ is the mean velocity profile, u_i the velocity fluctuation, p the pressure fluctuation, and ρ the density. If the right-hand side of this equation is assumed to be known then a compatible pressure field is found from the elliptic Poisson equation. Several investigators have solved this equation for the wall pressure using model terms on the right-hand side. The models have included only the turbulence-mean shear term because estimates of the turbulence–turbulence terms (Kraichnan 1956; Lilley & Hodgson 1960; Lilley 1964; Hodgson 1962) reveal that they contribute only about 5 % to the mean square pressure. This contribution is fairly uniform across the spectrum according to Hodgson (1962).

Kraichnan's (1956) computations predicted that the wavenumber spectrum $\phi(k_1)$ would rise as k_1^2 for low wavenumbers. The convection assumption $\omega = k_1 U_c$ implies an ω^2 dependence for the frequency spectra if U_c is constant. Hodgson (1962) using a different approach produced a pressure spectrum which rises at about $\omega^{1.75}$ in the low frequency region. By resorting to the electronic computer Panton & Linebarger (1974) were able to use a complicated model of the turbulence-mean shear term and found a wavenumber dependence of $k_1^{1.6}$ at low wavenumbers. They argued on dimensional grounds that the convective velocity $U_c(k_1)$ would obey a logarithmic equation. Their spectrum in the frequency-domain increased as $\omega^{1.5}$. All of these model calculations begin with the pressure equation and assume the turbulence-mean shear term dominates. In these models the low frequencies are contributed by large eddies.

Bradshaw (1967) approached the problem from a different tack. Assuming that the low-frequency components originate in the outer irrotational flow, he employed the concept of an irrotational flow over a bumpy wall (Liepmann 1954). The wall moves at a convective speed U_c and is imagined to be located at the displacement surface. Using the Bernoulli equation Bradshaw showed that the pressure fluctuations in the flow obey the equation

$$-p/\rho = (U_\infty - U_c)\, u_1 + \tfrac{1}{2}(u_1^2 + u_2^2 + u_3^2).$$

Since $U_\infty - U_c$ is about $0{\cdot}05 U_\infty$ or greater, the first term dominates. Bradshaw then extended the well-known analysis of Phillips (1955) to conclude that the spectrum of u_1 and hence the spectrum of p should behave as ω^2 for small ω.

The effects considered above are incompressible phenomena. Ffowcs Williams (1965) argued that the pressure spectrum might contain a compressible component at very low frequencies. This contribution comes from waves where the frequency is much greater than the wavenumber times the speed of sound and consists of 'acoustic' waves from non-compact sources (source size/wavelength $\to \infty$) in the flow. The frequency spectrum containing this effect may have a finite value at zero frequency. It should be noted that Ffowcs Williams's arguments point out the possible behaviour of the spectrum based upon the assumption that pressure sources of all wavenumbers and all frequencies are present.

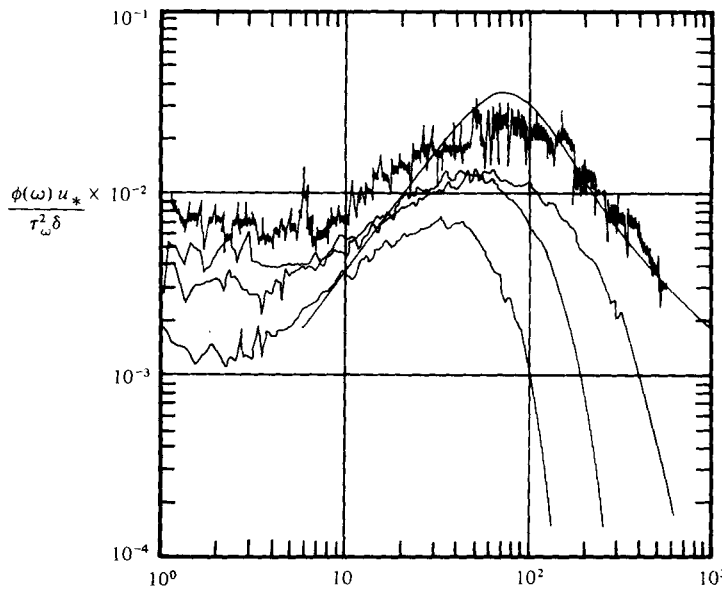

FIGURE 4. Power spectra of wall pressure for different size microphones. Lowest to highest curves are 1 in., $\frac{1}{2}$ in., $\frac{1}{4}$ in. and $\frac{1}{8}$ in. diameters. Smooth curve is model of Panton & Linebarger (1974).

Experimental verification of the low-frequency trends of the spectrum has proved to be a difficult task (as with the high frequency trends). Wind-tunnel measurements suffer from spurious acoustic noise, vibrations, free-stream turbulence, and in some cases secondary flows. For these reasons experimenters have been obliged to filter the low frequencies from their signals and concentrate on the mid-frequency results. The only experiments which have not been filtered are those made on sailplanes. Experiments on a glider wing by Hodgson (1962) conformed well to his model calculations showing a rising spectrum value with increasing frequency. Hodgson has questioned his results because there is a mild adverse pressure gradient on the wing (Hodgson 1971). Hodgson's (1971) more recent experiments (see Willmarth 1975*b*, figure 6) were made with a cuff around the wing to improve the pressure gradient. These experiments showed a constant level at low frequency. On the other hand, the model calculations of Panton & Linebarger (1974) show that adverse pressure gradients shift the level of the low- and mid-frequency spectrum without significant changes in the shape of the spectrum. Thus it is not likely that the difference between Hodgson's experiments can be explained by pressure gradient changes.

Measurements with different microphone diameters are given in figure 4 along with the model calculations. The different positions of high frequency fall off is the well-known effect of microphone diameter. The 1 in. diameter is so large that even at the peak frequency it is not measuring very much of the spectrum. The Corcos' size correction for microphones would double the peak value. At low frequencies all of the microphones have a plateau of different levels. It is believed that this is largely due to instrument noise.

The self noise of the microphones and how it depends upon microphone size will be discussed subsequently. First the influence of free-stream turbulence or acoustic

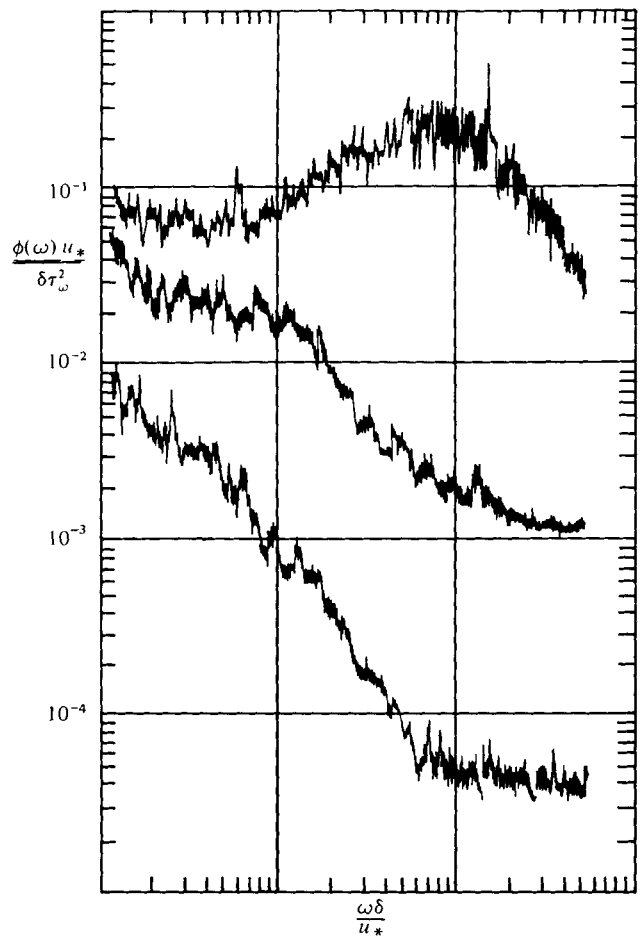

FIGURE 5. Power spectra of wall pressure (upper curve), free-stream microphone (middle curve), and free-stream hot wire (lower curve with arbitrary vertical scale).

contamination will be considered. At low frequencies the 1 in. microphone would measure any acoustic noise or large-scale convective fluctuations. The low level of the plateau for the 1 in. microphone allows us to rule out these phenomena as a substantial effect. This conclusion is supported by data from a hot wire and a microphone mounted in the free stream. The spectra of the free-stream microphone, hot wire, and a $\frac{1}{8}$ in. surface microphone are given in figure 5. Most of the signal on the free-stream microphone is induced 'noise' because of flow over the nose cone and turbulence in the free stream. The microphone nose cone that was employed in the flight tests has been replaced by a new design (B & K Model UA0386). The old cone has a blunt nose whereas the new design has a pointed nose. The flow induced noise is given by B & K (in 1974 Master Catalogue, p. 134) for the new design and has a shape similar to figure 5. Similar information for the old design is not available. The correlation coefficient between the hot wire and the free-stream microphone signals in figure 6 has maximum between 0·2 and 0·3. This shows a strong coupling between free-stream turbulence and the free-stream microphone measurements. Also shown in this figure are correlations with the

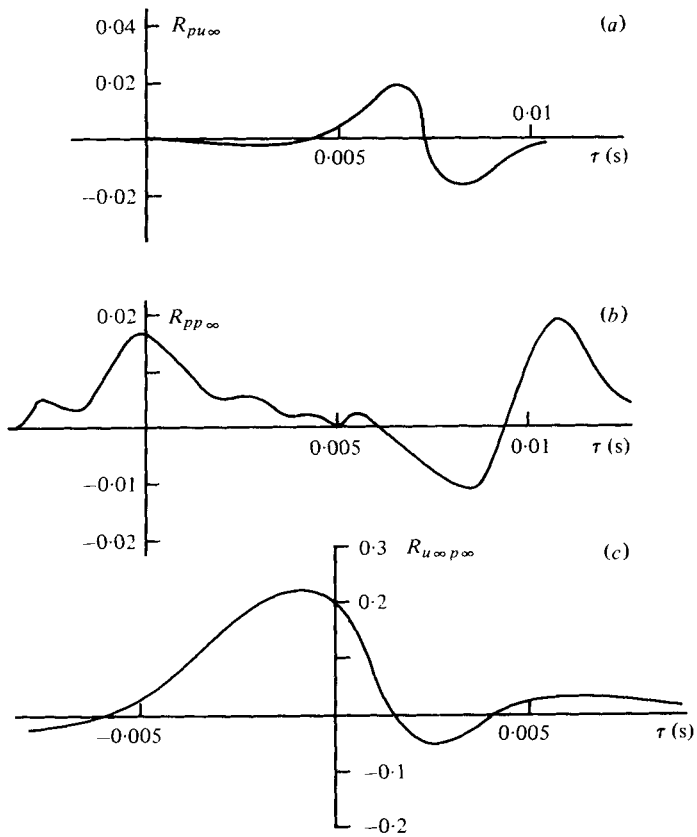

FIGURE 6. Correlation coefficients with time delay τ. (*a*) Wall pressure ($\frac{1}{8}$ in. microphone) and free-stream turbulence; (*b*) wall pressure and free-stream microphone; (*c*) free-stream turbulence and free-stream microphone. In each instance the second signal is delayed.

surface microphone which is 7·25 in. upstream of the hot wire and 8·75 in. upstream of the free microphone. The maximum correlation is a factor of 10 lower, about 0·02, for both the hot-wire and the free-stream microphone. Correlations at these lower levels could be picked out of the noise only by replaying the record so that effectively 80 s of record were correlated.

The microphones have two regions of correlation; one with a time delay associated with the convected turbulence and another with a nearly zero delay which must be an acoustic signal. The acoustic signal could be radiated sound produced by the boundary layer or noise from the entire glider flow field. In any event, the acoustic sound is not a significant part of the wall pressure. In order to verify that the sound was not concentrated at the low frequencies, as Ffowcs Williams speculated, the signals were filtered with a 5 Hz bandwidth filter and correlated again. The maximum values of this correlation were normalized by the r.m.s. intensities of the filtered signals and are shown in figure 7 as a function of frequency. From the data discussed above it is evident that sound, either radiated or ambient noise, and free-stream turbulence have a minimal contribution to the wall pressure. The signal from the free-stream microphone on the other hand shows a significant correlation with the face-stream turbulence and measures the small pressures associated with this turbulence.

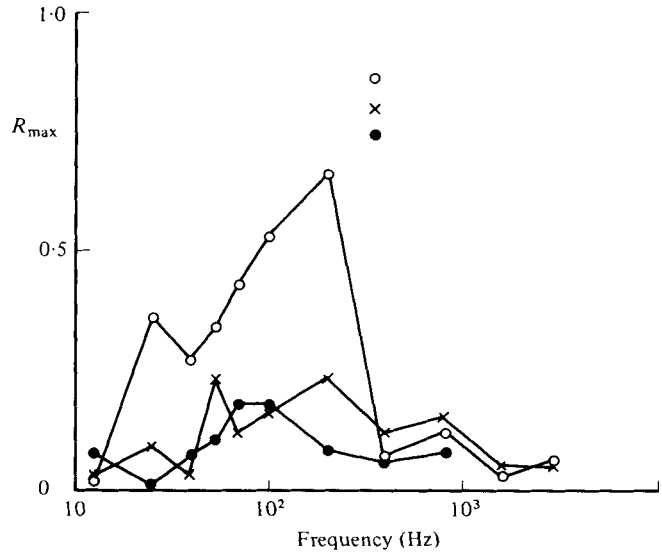

FIGURE 7. Maximum filtered correlations normalized by filtered r.m.s. values. ○, free-stream microphone and free-stream turbulence; ×, wall pressure and free-stream turbulence; •, wall pressure and free-stream microphone.

Figure 8 shows the results from some bench tests to determine the self-noise of the circuits and recording systems. The only difference in the bench system and the flight system was that an inverter was used to power the recorder whereas in the sailplane a battery pack was used. The inverter produced a 60 Hz spike which is evident on all signals. One test was made by shielding (with a pistonphone) the $\frac{1}{8}$ in. microphone from extraneous noise and making a recording. The spectrum of this noise shows a considerable magnitude at low frequencies. Another test was made in order to verify that self noise was influencing the microphones at low frequencies. In this test the preamplifier was terminated by a capacitance approximating (but not exactly equal to) that of a $\frac{1}{8}$ in. microphone. The object of this test was to eliminate the chance that low-frequency sound or vibration were passing through the shielding of the previous test and influencing the results. At extremely low frequencies the spectrum of this signal turned out to be even higher than the measured boundary-layer pressure. The third curve on figure 8 shows the flutter and noise characteristics of the tape recorder. The signal for this spectrum was obtained by recording with the input terminals of the tape recorder shorted. The fact that the tape recorder noise spectrum is significantly lower than the spectrum with a simulated microphone allows the conclusion that the microphone circuit is the major source of low-frequency noise.

There are two factors which cause the self-noise of a microphone to change with size. First the capacitance of the smaller microphones is less. This leads to more noise generated in the electronic preamplification circuit. Manufacturers data shows a 10-to-1 ratio of self-noise comparing the $\frac{1}{8}$ in. to the 1 in. microphones. Compounding the problem is the fact that the sensitivity of the microphones decreases with size. At a given acoustic input level small microphones require more amplification to produce the same signal and therefore yield a lower true signal-to-noise ratio of the recorded signals.

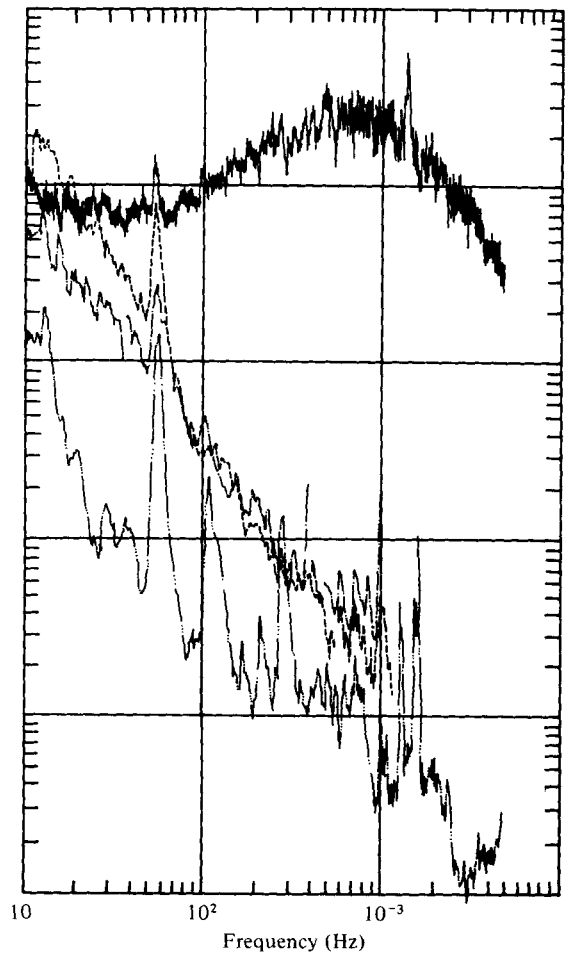

FIGURE 8. Spectra of instrumentation noise. ——, wall pressure; —·—, $\frac{1}{8}$ in. microphone self noise; – – –, simulated $\frac{1}{8}$ in. microphone self-noise; —· · ·—, tape recorder noise.

One additional piece of evidence supports the proposition that the plateau regions of figure 4 is caused by instrument self-noise. If the electronic noise is a constant level and the experiment is run at different airspeeds, then, in non-dimensional variables, the plateau will shift while the portion of the spectrum caused by boundary-layer pressures correlate. The ratio of plateau levels for a change in airspeed can be estimated by assuming that $\phi(\omega)$ is a constant value owing to instrument noise and that δ does not change

$$\frac{\left(\dfrac{\phi(\omega)\,u_*}{\tau^2\delta}\right)_{55}}{\left(\dfrac{\phi(\omega)\,u_*}{\tau^2\delta}\right)_{60}} \sim \frac{u_*^3]_{60}}{u_*^3]_{55}} \sim \frac{U_\infty^3]_{60}}{U_\infty^3]_{55}} = 1{\cdot}30.$$

The fact that δ does not change with airspeed was verified in the preliminary boundary-layer studies. The thinning of the boundary layer from increased speed was compensated by a forward movement of the transition position. Figure 9 gives results for the $\frac{1}{4}$ in. microphone at airspeeds of 55, 60 and 65 m.p.h. Even with these modest changes in

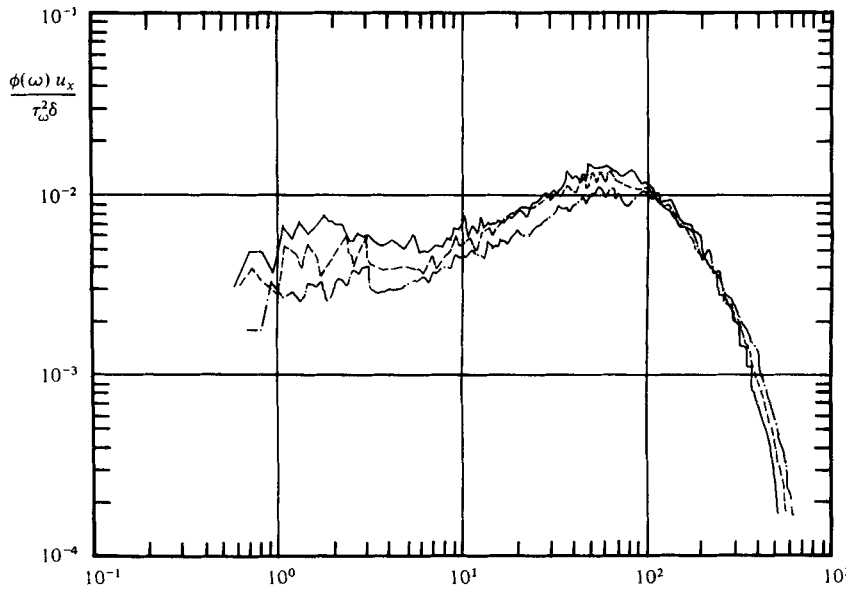

FIGURE 9. Change in plateau level with airspeed; ——, 55 m.p.h.; — —, 60 m.p.h.; —·—, 65 m.p.h.

airspeed there is a tendency for the plateau region to shift. If one assumes a level of 4·5 for the 60 m.p.h. plateau then the formula above produces levels of 5·85 and 3·55 for airspeeds of 55 and 65 m.p.h. respectively.

In order to establish that the measurements were independent of the location of the microphone in the constant pressure region, a flight was made with five microphones. Spectra from microphones located forward (20 in.), aft (10 in.), and to each side (4 in.) of the primary location (station 83·5) were found to compare very favourably with each other.

After the flights to obtain single point pressure spectra were completed a series of flights was conducted to obtain pressure–pressure and pressure–velocity correlations. Space-time correlations of pressure were obtained using an array of six $\frac{1}{8}$ in. microphones which were arranged over a span of 8·4 in. forward of station 83·4. Figure 10 gives the space–time correlations from these microphones. The shape and values agree substantially with the previous measurements of Willmarth & Wooldridge (1962) and those of Bull (1963). This supports these authors contention that high pass filtering does not appreciably affect their correlation data. There is no evidence of acoustic sound, which would appear as a positive hump at zero time delay, in these correlations.

Another point of interest is the existence of two time scales in the decay rates; an extremely rapid initial drop in the peak values followed by much longer, gentle decay. Blackwelder & Kovasznay (1972) observed a similar pattern for the velocity components in the outer portion of a boundary layer. The long decay is associated with the convection of large-scale structures. Figure 11 shows the decay of the maximum correlations for the wall pressure and for R_{vv} at $y/\delta = 0{\cdot}83$. Equations fitted to these cuves are

$$R_{pp\ \max} = 0{\cdot}36 \exp(-T/7{\cdot}5) + 0{\cdot}65 \exp(-T/1{\cdot}25),$$

$$R_{vv\ \max} = 0{\cdot}76 \exp(-T/6{\cdot}34) + 0{\cdot}24 \exp(-T/1{\cdot}15),$$

where $T = U_\infty \tau/\delta$.

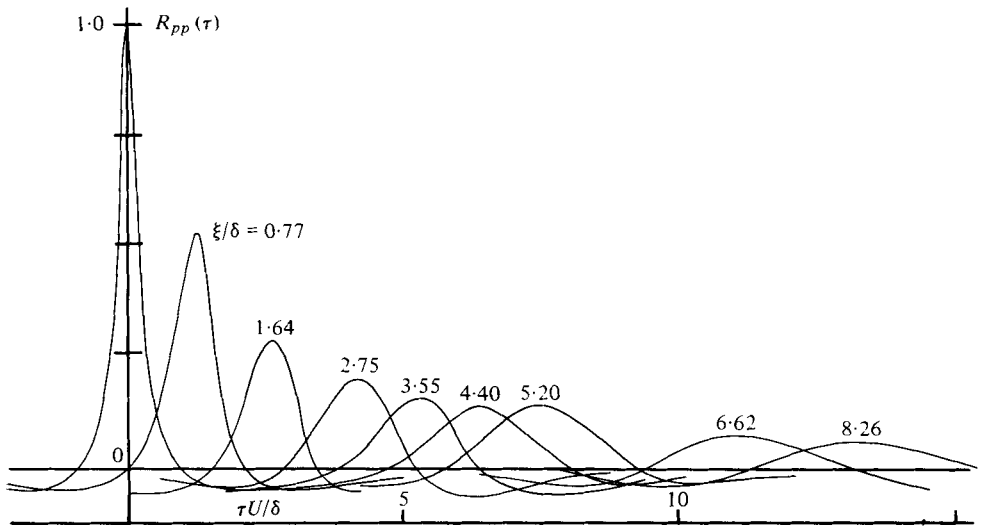

FIGURE 10. Pressure–pressure space–time correlations $R_{pp}(\tau)$. Distance between microphones are ξ/δ = 0, 0·77, 1·64, 2·25, 3·35, 4·40, 5·20, 6·62 and 8·26. Time-scale conversions are:

$$10\tau U/\delta = 0{\cdot}4\tau u_*/\delta = 65\tau U/\delta^*.$$

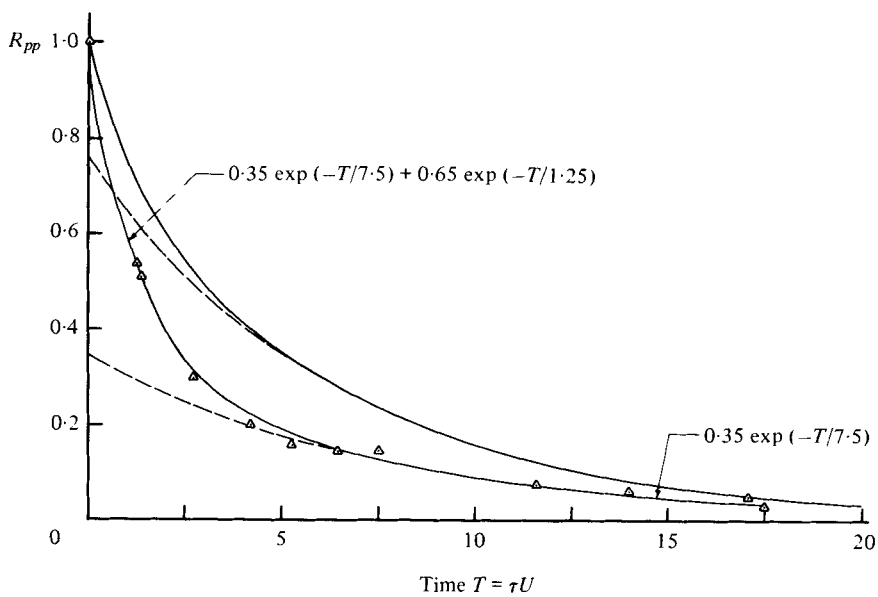

FIGURE 11. Maximum space–time correlations. Upper curves R_{vv} from Blackwelder & Kovasznay (1972), lower curves R_{pp} from figure 10.

The short decay time (exponential folding time) is about $T = 1{\cdot}2$ while the long decay time is $T = 7$. The R_{vv} equation is taken from Blackwelder & Kovasznay (1972). They interpret the intercept of the large-eddy component of the equation, 0·76, as the fraction of v energy due to large-scale motion in the turbulence. By similar reasoning the mean square pressure contains only a 35% contribution from the permanent

Nominal x-wire position	2 in.	1·5 in.	1 in.	0·8 in.	0·4 in.
Turbulence intensity as a % of free stream	0·19	0·45	2·4	3·4	4·8
Intermittency	0	0·01	0·48	0·96	1·0
$\bar{I}_{t++}$	0	0	0·10	0·16	0·17
$\bar{I}_{t+-}$	0	0	0·12	0·38	0·36
$\bar{I}_{t-+}$	0	0	0·16	0·27	0·30
$\bar{I}_{t--}$	0	0	0·10	0·15	0·16
$\bar{I}_{nt++}$	0·22	0·20	0·13	~ 0	0
$\bar{I}_{nt+-}$	0·27	0·28	0·25	0	0
$\bar{I}_{nt-+}$	0·28	0·27	0·07	0	0
$\bar{I}_{nt--}$	0·23	0·25	0·06	0	0

TABLE 2

large-eddy component. The fast-scale contributions to the pressure, from smaller-scale motions, and also from short time processes which change the shape of the large eddies, account for the largest component of the pressure.

5. Pressure–velocity correlations

Pressure–velocity correlations were measured with an x wire located slightly behind ($\frac{3}{8}$ in.) the surface microphone. The x wire was positioned remotely at different distances from the wall so that data at a sequence of positions could be obtained on a single flight. Five nominal positions both inside and outside the boundary layer were tested. The turbulence intensities and intermittency factors are given in table 2. There is some uncertainty about the location of the x wire from the wall because the traverse motor would slip upon occasion. The turbulent intensities and intermittency data indicate that the probe was nearer the wall than intended. It is probably best to interpret the data with reference to the intermittency.

The correlation coefficient $R_{uv}(\tau)$ is shown in figure 12. In denoting the correlation coefficients the standard practice of using the second index as the time-lagged variable is used. The two outermost probe positions are in completely non-turbulent flow and u and v are 90 % out of phase, as one expects for potential flow over a bumpy wall. The duration of the correlation is about 0·005 s. This corresponds to a convected space scale of about 0·5 ft or nearly 8 δ. The character changes for probe positions located where turbulence exists. $R_{uv}(0)$ takes on progressively larger negative values indicative of the Reynolds stress. This figure is essentially in agreement with similar curves published by Tritton (1967) and Kovasznay, Kibens & Blackwelder (1970).

Pressure–velocity correlations are given in figures 13 and 14. Although the intensity of the velocity fluctuations in the non-turbulent regions is small, the fluctuations maintain a strong correlation with the wall pressure. The R_{pu} and R_{pv} correlations are 90° out of phase and have the expected shape according to the Bernoulli equation given previously for flow over a wavy wall. These shapes can be deduced by considering the changes in u, v and p as shown in figure 15. Consider the point marked a in figure 15(b) where u is positive and v is negative. The pressure in this region is negative so P_{+-} will have a negative value at zero time delay. For time delays which are positive

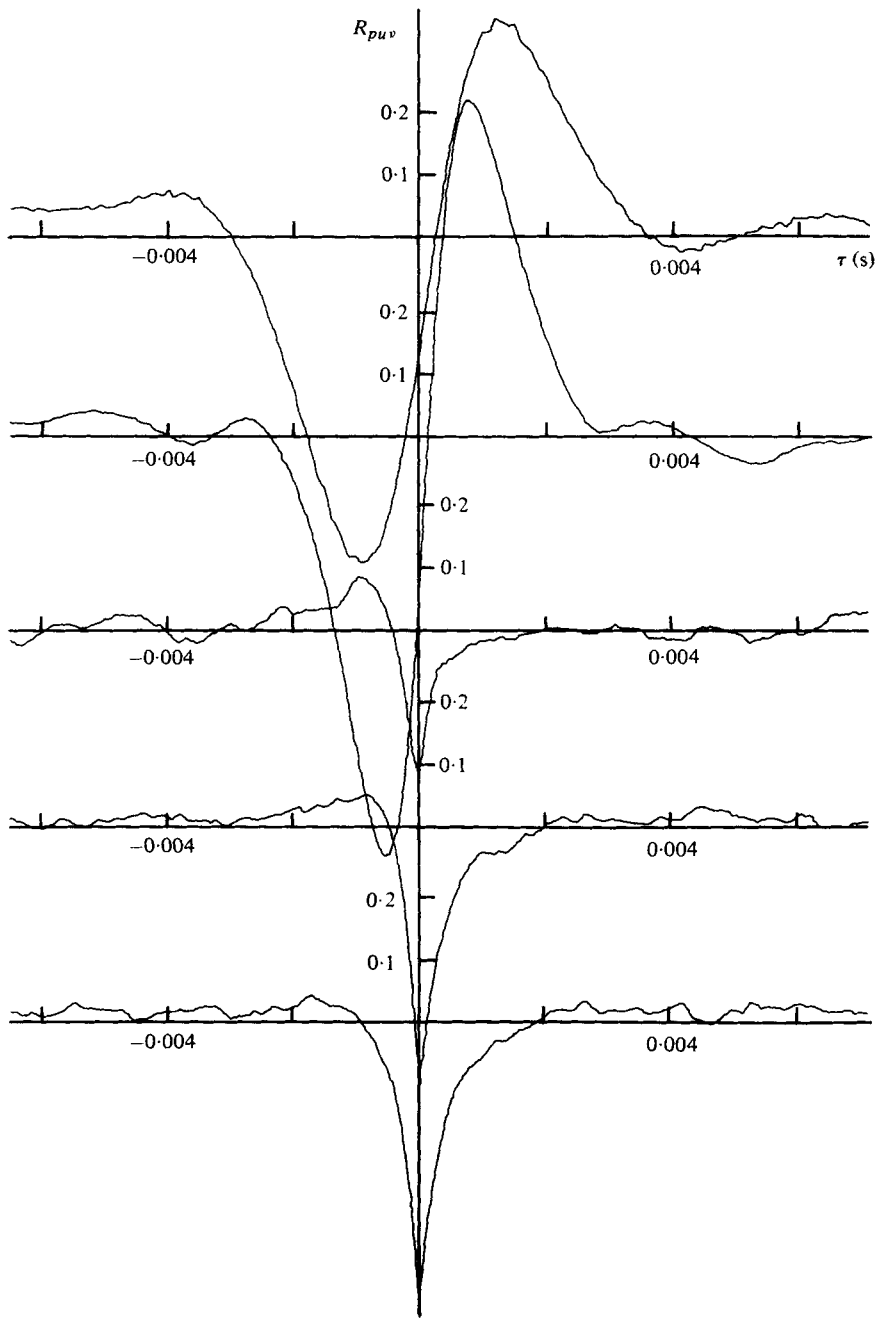

FIGURE 12. $R_{uv}(\tau)$ correlation coefficients at different positions in the boundary layer. From top to bottom nominal positions are y = 2, 1·5, 1, 0·8 and 0·4 in.

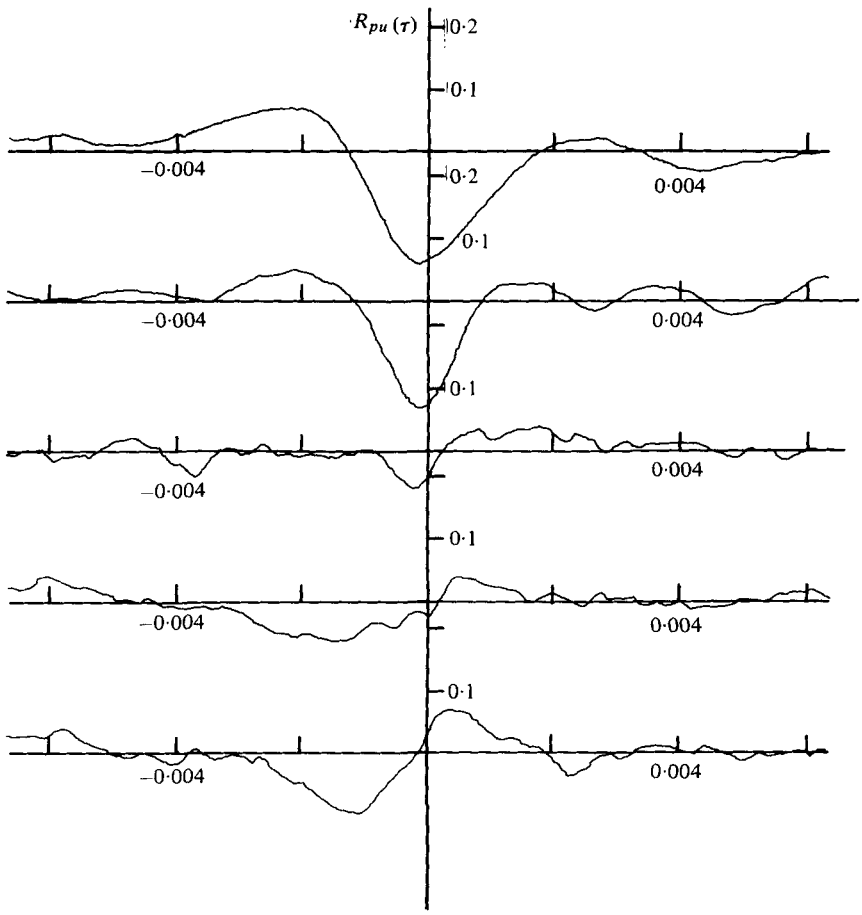

FIGURE 13. $R_{pu}(\tau)$ correlation coefficients. Positions same as figure 12.

the pressure and P_{+-} will tend to become positive as at point b in the figure. The opposite is true of point c which represents a negative time lag of the conditioning function with respect to the pressure.

To continue the discussion of figures 13 and 14 note that R_{pv} retains the same character for all probe locations except the time scale becomes shorter as the wall is approached. Willmarth (1975*a*) proposed a rotating vortex model of the large-eddy structure. He assumed a depressed pressure in the centre of the vortex and that flow outward from the wall would have a deficit in u while flow toward the wall would have an excess. The vortex model has the same p and v behaviour as the flow over the top of a wavy wall. The u velocity is not the same but is the opposite of the v characteristics. Thus one would expect the same type of R_{pv} correlation from either model and the measurements confirm this trend.

The R_{pu} correlations change their behaviour as the turbulent region is entered. At $y = 1$ in. the R_{pu} correlation retains the character of the irrotational motion although the intermittency is 0·48. On the other hand, the R_{uv} correlation at this point

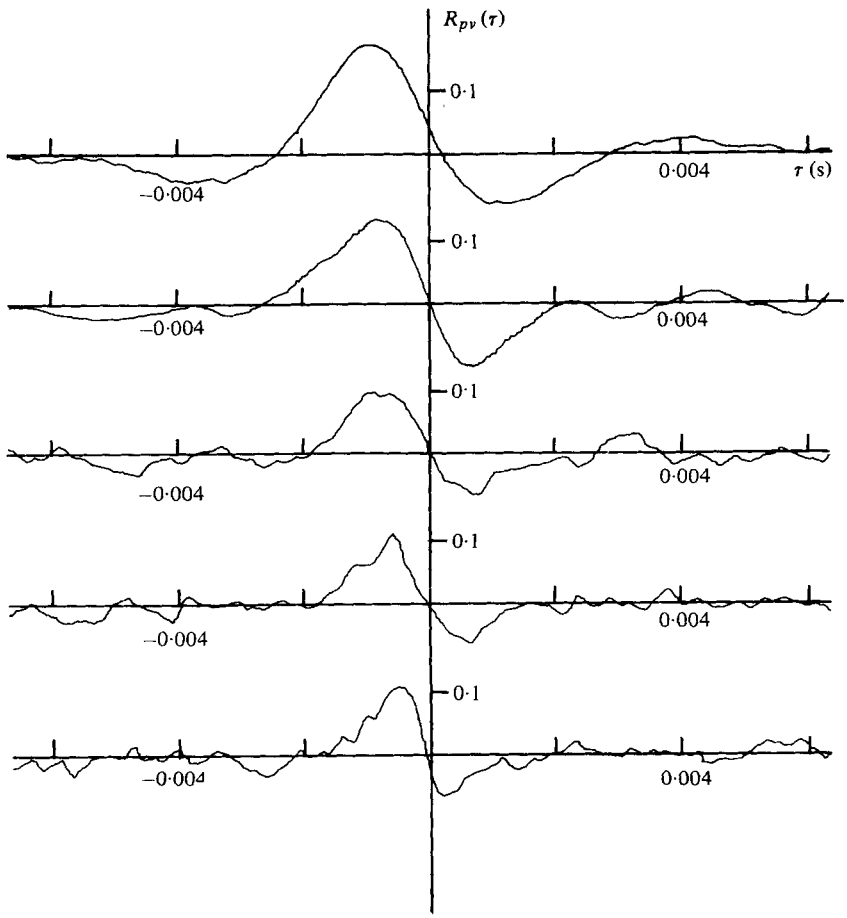

FIGURE 14. $R_{pv}(\tau)$ correlation coefficients. Positions same as figure 12.

has the character of the turbulent zone. At the two inner positions R_{pu} changes phase by 90° so that it is now 180° out of phase with R_{pv}. This change gives R_{pu} the character which would be expected of Willmarth's model. The final thing to note is that the scale of R_{pu} remains large as the wall is approached.

The last sequence of figures 16 and 17 attempts to gain further insight into the pressure field through conditional correlations. The velocity signals were first classified into turbulent and non-turbulent periods. The detection scheme used essentially the method of Hedley & Keffer (1974). The flow was called turbulent if the sum of the $\partial u/\partial t$ and $\partial v/\partial t$ exceeded a criterion value for a certain smoothing time. In order to fill in drop outs which occur at peaks where u and v change sign, the flow was also called turbulent if the sum of the second derivatives $\partial^2 u/\partial t^2$ and $\partial^2 v/\partial t^2$ exceeded a specified value. The constants for the detection criteria were determined by viewing the u, v and intermittency signals together. The next classification was made on the basis of the sign of u and that of v. For example, the conditioning signal I_{t+-} is one when turbulent flow with positive u and negative v occurs at the hot wire. One of the eight possible

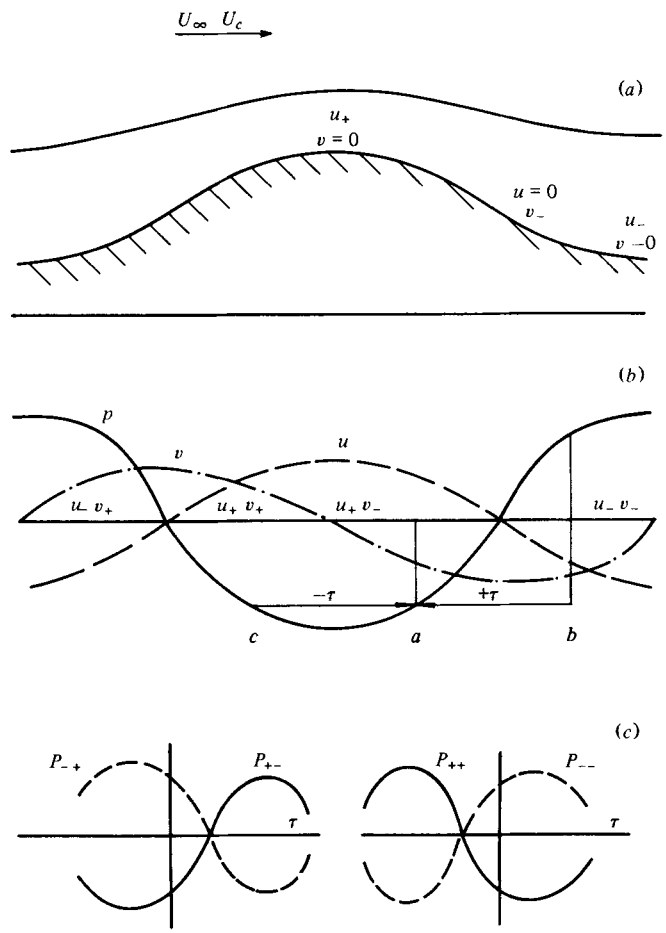

FIGURE 15. Irrotational flow over a wavy wall: (*a*) schematic; (*b*) flow variables; (*c*) corresponding conditional correlations of pressure,

conditioning signals is always one and the remaining seven are zero. Since the event which produces the pressure and the velocity event at the probe may not occur simultaneously we formed the lagged correlation of p and I as follows:

$$P_{nt}(\tau)_{+-} \equiv \frac{1}{p'(\bar{I}_{nt+-})^{\frac{1}{2}}} \overline{[\rho(t)\, I_{nt+-}(t+\tau)]}.$$

The intent is to find the average pressure connected with the conditioning event. The normalization factor is the r.m.s. value of p times the r.m.s. value of I. Because of the 0, 1 character of I, its r.m.s. value is also the square root of the average value $\bar{I}$.

The conditional correlations have the property that the sum of all correlations weighted by their respective $\sqrt{\bar{I}}$ factors is zero for any τ,

$$0 = \sum_{ijk} (\bar{I}_{ijk})^{\frac{1}{2}} p_{ijk}.$$

In this equation $i = t$ or nt, $j = +$ or $-$, $k = +$ or $-$ and the sum extends over all possible combinations. This relation follows from two facts: the sum of all conditioning indicators in unity and the average pressure is zero.

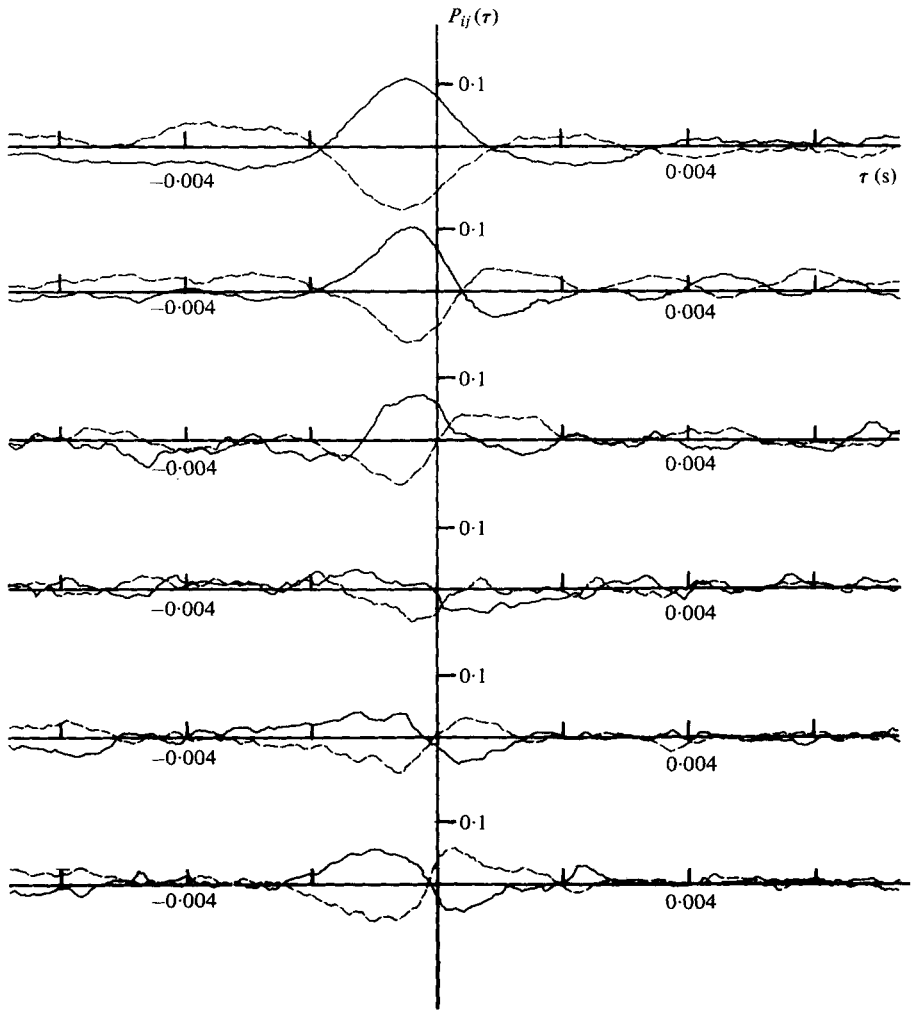

FIGURE 16. Conditional pressure correlations: ——, $P_{-+}(\tau)$; – – –, $P_{+-}(\tau)$. Positions across the boundary layer from top to bottom 2 in., 1·5 in., 1 in. non-turbulent, 1 in. turbulent, 0·8 in. and 0·4 in.

The average duration of the indicator signals $\bar{I}$ is given in table 2. When the flow is non-turbulent the motions are relatively evenly divided among the classifications. The completely turbulent flow on the other hand tends to favour motions where u and v are of opposite sign.

The correlation P_{+-} and P_{-+} tend to be complete opposites as do P_{++} and P_{--}. At the non-turbulent locations the curves have the trends that are expected for a wavy wall as depicted in figure 15. For the one-inch position sets of curves are given for both the turbulent and the non-turbulent periods. The turbulent period correlations are much smaller than the non-turbulent correlations. This is interpreted to mean that the irrotational motions are almost completely responsible for the contributions to the wall pressure from this position. Motions in the turbulent region are the superposition of vortical and irrotational fluctuations (Panton 1978). Because the conditioning

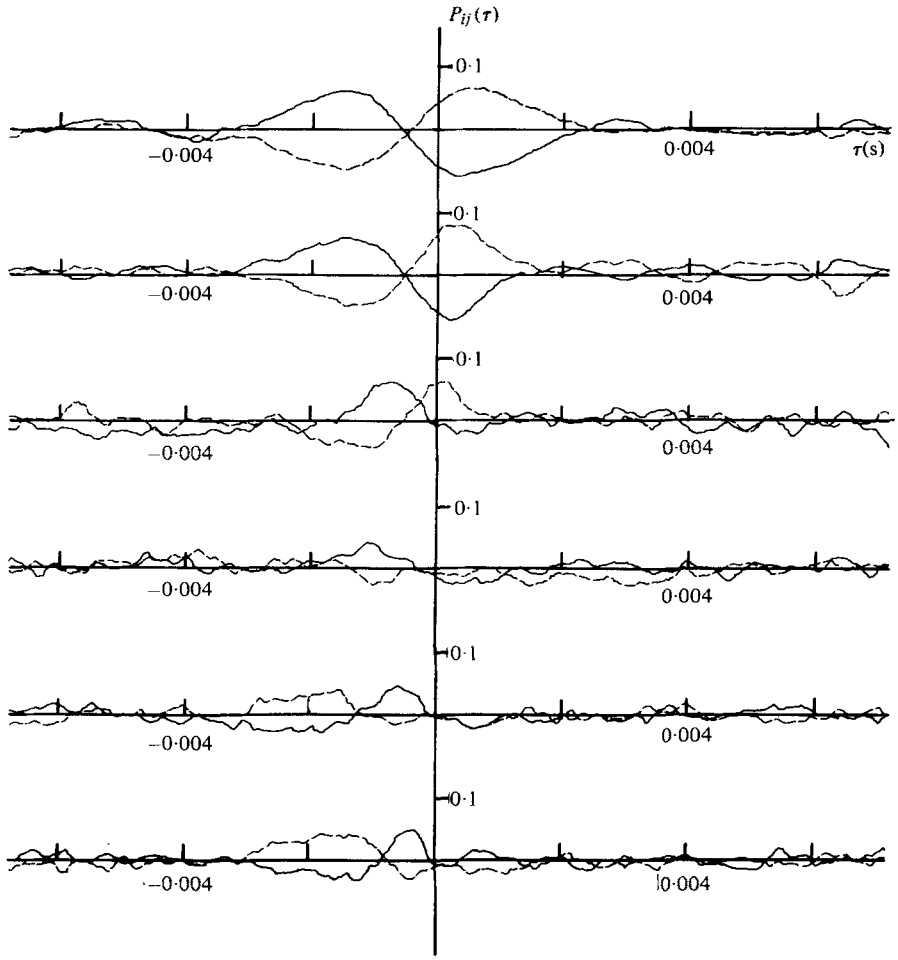

FIGURE 17. Conditional pressure correlations: ——, $P_{++}(\tau)$; – – –, $P_{--}(\tau)$. Positions across the boundary layer same as figure 16.

signal responds to the sign of the total velocity, irrotational plus vortical, the correlations are smaller in the turbulent region. The two completely turbulent positions near the wall have less well defined P_{++} and P_{--} correlations. The P_{+-} and P_{-+} curves appear more regular and have shifted phase with respect to the flow in the non-turbulent zone. The vortex model cannot be used to interpret the conditioned correlations as it does not have any $+ +$ or $- -$ motions.

6. Summary

Experiments with the sailplane offered a noise-free flow with a low free-stream turbulence level. In this environment the wall-pressure spectrum of a turbulent boundary layer with natural transition was found to drop off at low frequencies. This behaviour is in agreement with model calculations based on the turbulence-mean shear term as the dominating mechanism. Correlations between several wall-mounted microphones showed that the large-scale motions contribute about 35 % to the mean

square pressure. These contributions come not only from the turbulent region but also from the unsteady non-turbulent region. Maximum $R_{pu}(\tau)$ and $R_{pv}(\tau)$ correlations above 0·15 were observed with a hot wire mounted outside the boundary layer where the fluctuations were completely irrotational. The time-lagged correlations have the character of a potential flow over a convected bumpy wall. The length scale associated with these correlations is about 8 times the boundary-layer thickness. When the hot wire was at the 50 % intermittency level in the boundary layer, the non-turbulent motions had a larger correlation with the wall pressure than did the turbulent motions. This leads to the conjecture that the irrotational motions in the turbulent region are primarily responsible for the large-scale wall-pressure fluctuations. A time-lagged conditional correlation of the pressure was introduced in order to gain further insight into the pressure producing motions. This function indicates the average wall pressure, after a time lag τ, during time periods when the velocity components u and v have a specified sign. The conditional correlations for $u-, v+$ are almost exactly the negative of those for $u+, v-$. A similar statement may be made about $u-, v-$ and $u+, v+$ correlations. These trends were observed at all measurement positions in the boundary layer.

The work reported here was supported by the NASA Ames Research Center through grants NGR 37-002-083, NGR 44-012-221 and NSG-2189. This support is gratefully acknowledged.

REFERENCES

BAKEWELL, H. P. 1968 *J. Acoust. Soc. Am.* **43**, 1358.

BENDAT, J. S. & PIERSOL, A. G. 1971 *Random Data: Analysis and Measurement Procedures.* Wiley Interscience.

BLACKWELDER, R. F. & KOVASZNAY, L. S. G. 1972 *Phys. Fluids* **15**, 1545.

BRADSHAW, P. 1967 *J. Fluid Mech.* **27**, 209.

BULL, M. K. 1963 *AGARD Rep.*, 455.

COLES, D. E. & HIRST, E. A. 1968 *Proc. Conf. on Computation of Turbulent Boundary Layers, Stanford, Ca.* vol. II.

FFOWCS WILLIAMS, J. E. 1965 *J. Fluid Mech.* **22**, 507.

HEDLEY, T. B. & KEFFER, J. F. 1974 *J. Fluid Mech.* **64**, 625.

HODGSON, T. H. 1962 Ph.D. Thesis, University of London.

HODGSON, T. H. 1971 *Proc. 1st Interagency Symp. on Transportation Noise, Purdue Univ.*, p. 510.

KOVASZNAY, L. S. G., KIBENS, V. & BLACKWELDER, R. F. 1970 *J. Fluid Mech.* **41**, 283.

KRAICHNAN, R. H. 1956 *J. Acoust. Soc. Am.* **28**, 378.

LIEPMANN, H. W. 1954 *GALCIT/N.A.C.A. Contract Rep.* NAW-6288 (*Aero. Res. Counc.* no. 23515, 1962).

LILLEY, G. M. 1964 *Arch. Mech. Stosow.* **16**, 301.

LILLEY, G. M. & HODGSON, T. H. 1960 *AGARD Rep.*, 276.

PANTON, R. L. 1978 *J. Fluid Mech.* **88**, 97.

PANTON, R. L. & LINEBARGER, J. H. 1974 *J. Fluid Mech.* **65**, 261.

PHILLIPS, O. M. 1955 *Proc. Camb. Phil. Soc.* **51**, 220.

TRITTON, D. J. 1967 *J. Fluid Mech.* **28**, 439.

WILLMARTH, W. W. 1975*a* *Adv. Appl. Mech.* **15**, 159.

WILLMARTH, W. W. 1975*b* *Ann. Rev. Fluid Mech.* **7**, 13.

WILLMARTH, W. W. & WOOLDRIDGE, C. E. 1962 *J. Fluid Mech.* **14**, 187.

WILLMARTH, W. W. & YANG, C. S. 1970 *J. Fluid Mech.* **41**, 47.

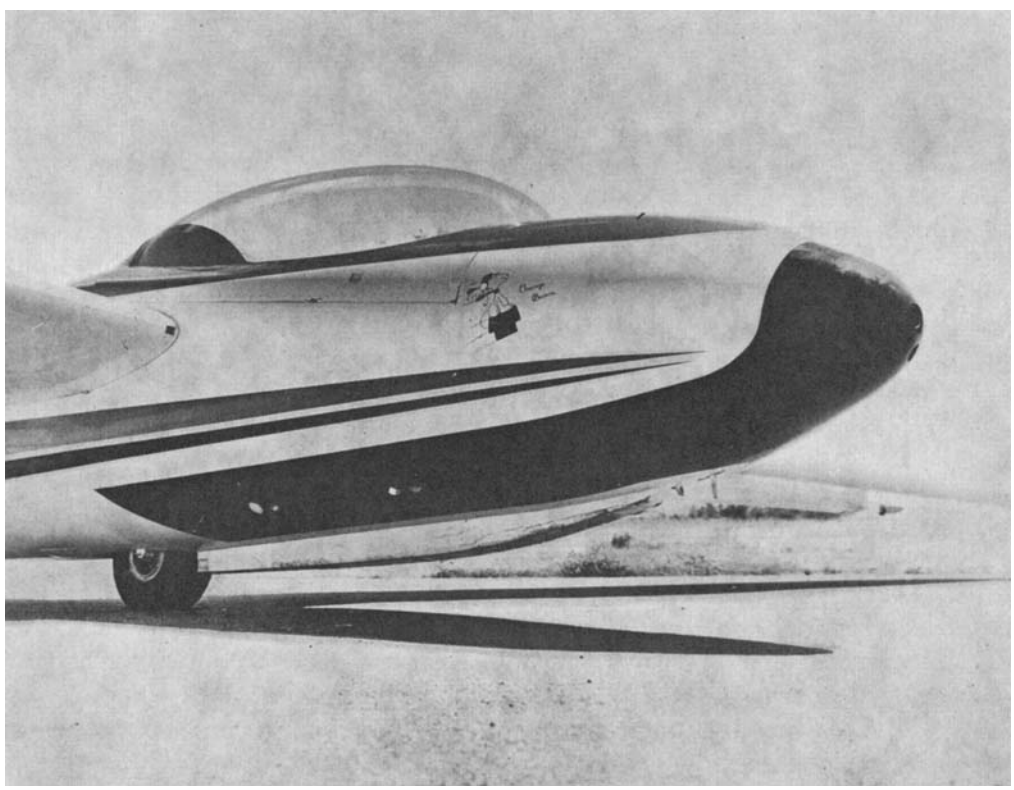

FIGURE 1. Schweizer 2-32 sailplane showing region on the lower fuselage where measurements were made.